Poiseuille flow; good agreement between experiment and inviscid theory is reported.

Velocity distributions in the impinging jet were measured for nozzle-to-surface distances of 0.5 and 1.0R. Except for the boundary layer regions close to the impingement surface and at the edge of the jet, the velocity data are independent of Reynolds number, demonstrating the inviscid nature of the jet.

Pressure distributions on the impingement surface were measured for nozzle heights in the range 0.1 to 12R. The data for $H/R \geqq 1.0$ show no significant dependence on either Reynolds number or nozzle height. For $H/R < 1.0$ the effect of flow constriction between the nozzle and the surface becomes apparent as the nozzle wall is approached. Close to the stagnation point, $x/R << 1$, flow is, however, not influenced by nozzle height in the range tested. The flow constriction results in a pressure loss which increases rapidly with decreasing H/R.

ACKNOWLEDGMENT

Financial assistance from the National Research Council of Canada is gratefully acknowledged.

NOTATION

A_{2n} = constant coefficients in inviscid solution
$C_n^{3/2}(\mu)$ = Gegenbauer polynomial
D = nozzle diameter, ft.
g_c = gravitational conversion factor, lb.$_m$-ft./lb.$_f$-sec.^{2}
h = normal distance from surface, ft.
H = nozzle-to-surface distance, ft.
$\vec{i}_\phi$ = unit vector
p = pressure, lb.$_f$/sq. ft.
p_A = ambient pressure, lb.$_f$/sq. ft.
p_N = pressure inside nozzle, lb.$_f$/sq. ft.
$\mathcal{P}_n(\mu)$ = Legendre function of the first kind
r = spherical polar coordinate
R = nozzle radius, ft.
$\mathcal{R}_n(\mu)$ = function defined by Equation (23)
U_N = velocity maximum in nozzle, ft./sec.
U_B = velocity along free streamline
$\overline{U}$ = average velocity in nozzle, ft./sec.
$\vec{V}$ = velocity vector, ft./sec.
V = velocity
v_r = velocity component in r direction
v_θ = velocity component in θ direction
v_ϕ = velocity component in ϕ direction
x = radial distance along surface, ft.

Greek Letters

β = pressure loss coefficient, Equation (31)
δ = boundary layer thickness, ft.
Δ = value of h on free boundary
Δp = dimensionless pressure
$\vec{\zeta}$ = vorticity vector
θ = spherical polar coordinate
μ = cos θ
ν = kinematic viscosity, sq. ft./sec.
ρ = density, lb./cu. ft.
ϕ = spherical polar coordinate
ψ = stream function

Dimensionless groups

N_{Re} = Reynolds number = $\overline{U}D/\nu$

LITERATURE CITED

1. Brady, W. G., and G. Ludwig, *Inst. Aerospace Sci., Paper No. 63-29* (1963).
2. Leclerc, A., M.Sc. Thesis, State Univ. Iowa (1948).
3. Ranz, W. E., and P. F. Dickson, Univer. Minnesota, private communication (1962).
4. Schach, W., *Ing. Archiv.*, **6**, 51 (1935).
5. Shen, Y. C., *Inst. Aerospace Sci., Paper No. 62-144* (1962).
6. Strand, T., *Am. Inst. Aeron. Astronaut paper No. 64, 424* (1964).
7. Gardon, R., and J. Cahit Akfirat, *Intern. J. Heat Mass Transfer*, **8**, 1261 (1965).
8. Sutera, S.P., P. F. Maeder, and J. Kestin, *J. Fluid Mech.*, **16**, 497 (1963).
9. Rao, V. V., and Olev Trass, *Can. J. Chem. Eng.*, **42**, 95 (1964).
10. Dawson, D. A., and O. Trass, *ibid.*, **44**, 121 (1966).
11. Schrader, H., *VDI-Forsh. -Heft.*, 484, Düsseldorf (1961).
12. Milne-Thomson, L. M., "Theoretical Hydrodynamics," 3rd Ed., p. 527, Macmillan and Co., London, (1956).
13. Crandel, S. H., "Engineering Analysis: A Survey of Numerical Procedures," McGraw-Hill, New York (1956).
14. Scholtz, M. T., Ph.D. dissertation, Univ. Toronto, (1965).
15. Schlichting, H., "Boundary Layer Theory," 4th Ed., McGraw-Hill, New York (1960).
16. Glauert, M. B., *J. Fluid Mech.*, **1**, 625 (1956).
17. Scholtz, M. T. and O. Trass, *AIChE J.*, **9**, 548 (1964).

Part II. Boundary Layer Flow-Mass Transfer

Exact solutions of the boundary layer equations were used to calculate the local mass transfer coefficients for an impinging jet with a parabolic velocity distribution. Boundary conditions were obtained from an inviscid flow solution and also from experimental pressure distributions. Experimental data for the air/naphthalene system were in good agreement with theoretical results. Mass transfer from the impingement surface was independent of nozzle height in the range 0.5 to 12 nozzle radii. For lower nozzle heights the effect of the constriction of flow between the nozzle and the surface led to increased transfer rates near the nozzle wall; data followed the predicted behavior.

Part I of this paper deals with that region of the flow of an impinging nonuniform jet which can be considered to be external to viscous boundary layers. In this part of the paper the viscous boundary layer on the impingement surface, characterized by the impingement flow of Part I, is examined.

The viscous boundary layer which develops on the impingement surface is initially laminar, although transition to a turbulent boundary layer may occur some distance from the stagnation point. Brady and Ludwig (*1*) made experimental velocity measurements in the boundary layer of the turbulent uniform impinging jet and these were compared with velocity profiles calculated using experimental pressure distribution data; the critical radial distance from the stagnation point for neutral boundary layer stability was also calculated. From their measurements it was concluded that significant penetration of turbulence into the laminar boundary layer does occur for radial dis-

tances less than the critical radius; for a nozzle Reynolds number of 1.2×10^6, however, the boundary layer out to 1.4 nozzle radii was distinctly laminar.

The present problem, therefore, deals only with a laminar boundary layer in the stagnation region; no turbulent perturbation of the boundary layer is considered. The results of this study provide a theoretical prediction as well as experimental verification of mass transfer in a turbulence-free, nonuniform jet; such fundamental results should aid in the independent evaluation of the effects of variables such as turbulence, roughness and erosion in other impinging jet studies.

THEORETICAL

In cylindrical coordinates the continuity and boundary layer equations for axisymmetric flow, assuming constant fluid properties and low mass transfer rates, are:

continuity,

$$\frac{\partial(ux)}{\partial x} + \frac{\partial(vx)}{\partial y} = 0 \tag{1}$$

momentum,

$$u\frac{\partial u}{\partial x} + v\frac{\partial u}{\partial y} = -\frac{1}{\rho}\frac{dp}{dx} + \nu\frac{\partial^2 u}{\partial y^2} \tag{2}$$

mass diffusion,

$$u\frac{\partial c}{\partial x} + v\frac{\partial c}{\partial y} = \mathcal{D}\frac{\partial^2 c}{\partial y^2} \tag{3}$$

Before prescribing the boundary conditions to be satisfied by the solutions of these equations it is necessary to examine the conditions at the outer edge of the boundary layer as determined by the inviscid flow of Part I of this paper.

Neglecting the thickness of the boundary layer on the impingement surface, the velocity along this surface is obtained from Part I in the form:

$$\frac{U(x)}{U_N} = \sum_{n=1}^{\infty} A_{2n}\left(\frac{x}{R}\right)^{2n-1} \mathcal{R}'_{2n}(0) \tag{4}$$

or more generally,

$$U(x) = \sum_{n=1}^{\infty} u_{2n-1}x^{2n-1} \tag{5}$$

The coefficients A_{2n} are tabulated in Part I for nozzle-to-surface distances of 0.1, 0.25, 0.375, 0.5, and 1.0 nozzle radii. The vorticity at the deflecting surface from Part I is:

$$\vec{\zeta} = -2x \tag{6}$$

In order that the boundary layer and inviscid solutions be compatible at the edge of the boundary layer, both Equations (4) and (6) must be satisfied as boundary conditions. It is recalled from Part I, however, that the vorticity in what can be considered the inviscid region of the jet is of much lower order than in the boundary layer; for purposes of the boundary layer solution the limiting value of the vorticity, as $y \to \infty$, will be assumed zero. The boundary conditions can now be written:

$$y = 0; \quad u = v = 0, \quad c = c(x, 0) \tag{7}$$

$$y \to \infty; \quad u \to U(x), \quad \frac{\partial u}{\partial y} \to 0, \quad c \to c(x, \infty) \tag{8}$$

Considering the form of $U(x)$ given by Equation (5), the boundary condition (8) $u \to U(x)$, precludes the possibility of a solution based on boundary layer similarity. For larger radial distances either approximate numerical boundary layer calculations or an exact series solution of the boundary layer equations must be used.

For the present problem of axisymmetric stagnation flow on a plane surface the series expansion method has been chosen. This solution method, due to Blasius has been applied by Boltze and Froessling to blunt bodies of revolution and the first four terms of the series have been evaluated (2). Froessling has also applied the method of series expansion to the thermal boundary layer equation for blunt bodies of revolution and evaluated the first two terms for a Prandtl number of 0.7. "Boundary Layer Theory" by H. Schlichting gives an excellent account of the series expansion methods and their applications (2).

The numerical calculations which extend the series expansion solution of the momentum and diffusion boundary layer equations to seven terms for the axisymmetric stagnation flow on a plane surface have been done by Scholtz (3); solutions for Schmidt numbers in the range 0.7 to 2,000 are tabulated in this reference. An approximation to the concentration gradients at the wall has been derived from the exact series solution and a method for making mass transfer calculations for all Schmidt numbers in the range 0.7 to 2,000 is given.

The essential steps involved in using the boundary layer solutions from reference 3 to obtain velocity profiles and mass transfer coefficients for the present nonuniform jet are given here, but in order to follow the details of the procedure, either reference 2 for the general procedure or (3) for the specific calculations is necessary.

Solution of the Momentum Equation

The pressure gradient in the radial direction is impressed on the boundary layer by the inviscid flow, giving, from Equation (4):

$$-\frac{dp}{dx} = U(x)\frac{dU(x)}{dx} \tag{9}$$

A stream function ψ is defined such that:

$$u = \frac{\partial\psi}{\partial y} \tag{10}$$

and

$$v = -\left(\frac{\partial\psi}{\partial x} + \frac{\psi}{x}\right) \tag{11}$$

Following (2), the stream function may be written,

$$\psi(x, y) = \sqrt{\frac{\nu}{2u_1}}\{u_1 x f_1(\eta) + 2u_3 x^3 f_3(\eta) + \ldots + 7u_{13}\, x^{13} f_{13}(\eta)\} \tag{12}$$

where:

$$\eta = y\sqrt{\frac{2u_1}{\nu}} \tag{13}$$

The coefficients u_1, u_3 in Equation (12) are given by Equations (4) and (5); the functions $f_1(\eta)$, $f_3(\eta)$ .... $f_{13}(\eta)$ are calculated using the boundary layer solution given elsewhere (3).

Noting that $\mathcal{R}_2'(0) = -1/2$, from Equations (4), (5), and (13),

$$\eta = (-A_2)^{1/2}\left(\frac{y}{R}\right) N_{Re}^{1/2} \tag{14}$$

and from Equations (4), (10), and (12), replacing the $\mathcal{R}'_{2n}(0)$ by their numerical values gives the boundary layer velocity profile:

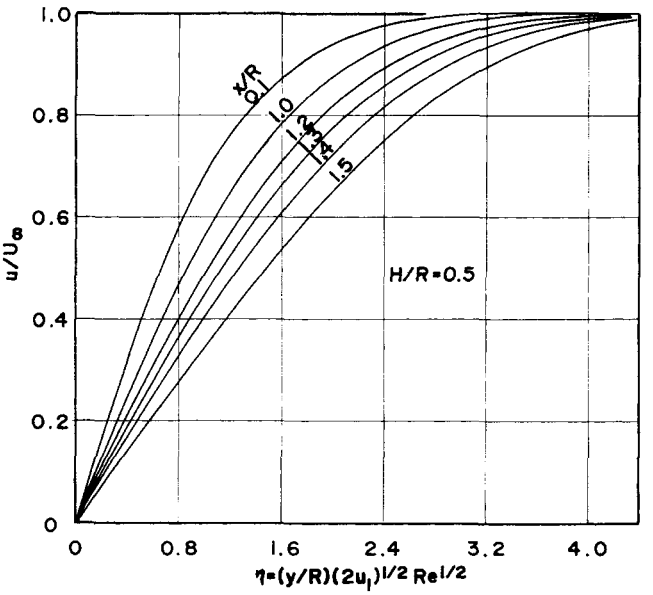

Fig. 1. Velocity profiles in boundary layer on impingement surface, $H/R = 0.5$.

$$\frac{u}{U_N} = \frac{-A_2}{2} f_1'(\eta)\left(\frac{x}{R}\right) + \frac{6}{8} A_4 f_3'(\eta)\left(\frac{x}{R}\right)^3 + \ldots. \frac{-63{,}063}{43{,}008} A_{14} f'_{13}(\eta)\left(\frac{x}{R}\right)^{13} \quad (15)$$

Equation (15) is a general expression for the boundary layer velocity profile characterized by the nonuniform impinging jet. The coefficients A_2, A_4, ... have been calculated and are tabulated in Part I of this paper for nozzle-to-surface distances of 0.1, 0.25, 0.375, 0.5, and 1.0 nozzle radii.

Following the method of calculating the functions $f'_1(\eta), f'_3(\eta)$ .... $f'_{13}(\eta)$ given elsewhere (3), the boundary layer velocity profiles for $H/R = 0.5$ have been calculated. Profiles for intervals of x between $0.1R$ and $1.5R$ are shown in Figure 1.

Very close to the stagnation point of the jet only the first term of Equation (15) need be considered and the boundary layer solution reduces to the stagnation flow solution of Homann (2). Homann's exact solution of the Navier-Stokes equations includes a free constant which in the present case takes the value u_1; Homann's solution shows that the boundary layer thickness is independent of radial distance x. The velocity profile in Figure 1 for $x/R = 0.1$ closely approximates Homann's solution. For larger radial distances the higher order terms in Equation (15) are required to describe the flow, and the boundary layer thickness is seen from Figure 1 to increase with distance from the stagnation point.

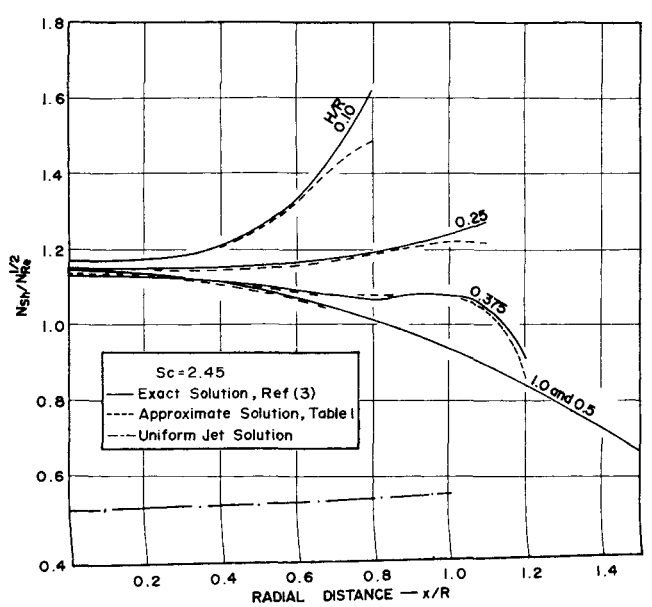

Fig. 2. Predicted mass transfer from impingement surface, $0.1 \leq H/R \leq 1.0$, $N_{Sc} = 2.45$. Uniform and nonuniform jet.

SOLUTION OF THE MASS DIFFUSION EQUATION

A dimensionless concentration parameter is defined as

$$\bar{c}(x,y) = \frac{c(x,y) - c(x,\infty)}{c(x,0) - c(x,\infty)} \quad (16)$$

and the concentration of the diffusing species in the boundary layer may be written as

$$\bar{c}(x,\eta) = c_0(\eta) + c_2(\eta)x^2 + c_4(\eta)x^4 + \ldots. \quad (17)$$

A mass transfer coefficient, k, at the impingement surface ($y = 0$) is defined by

$$N_0 = k\,[c(x,0) - c(x,\infty)] = -\mathcal{D}\left.\frac{\partial c}{\partial y}\right|_{y=0} \quad (18)$$

giving

$$k = -\mathcal{D}\sqrt{\frac{2u_1}{\nu}}\,\frac{\partial \bar{c}\,(0)}{\partial \eta} \quad (19)$$

Substituting for u_1 and rearranging gives

$$\frac{N_{Sh}}{N_{Re}^{1/2}} = -(-A_2)^{1/2}\,[c'_0(\eta) + c'_2(\eta)\,x^2 + c'_4(\eta)\,x^4 + \ldots.] \quad (20)$$

Equation (20) is a general expression giving the Sherwood number in terms of the nozzle Reynolds number and radial distance from the stagnation point. To evaluate the functions $c'_0(\eta)$, $c'_2(\eta)$ ..... from the coefficients A_2, A_4 ... given in Part I involves considerable arithmetic. For example, the function $c'_4(\eta)$ is given in the literature (3) as:

$$c'_4(\eta) = \left[\frac{A_6\,\mathcal{R}'_6(0)}{A_2\,\mathcal{R}'_2(0)}\,d'_4(\eta) + \frac{A_4^2\,\mathcal{R}'^2_4(0)}{A_2^2\,\mathcal{R}'^2_4(0)}\,e'_4(\eta)\right]\frac{1}{R^4} \quad (21)$$

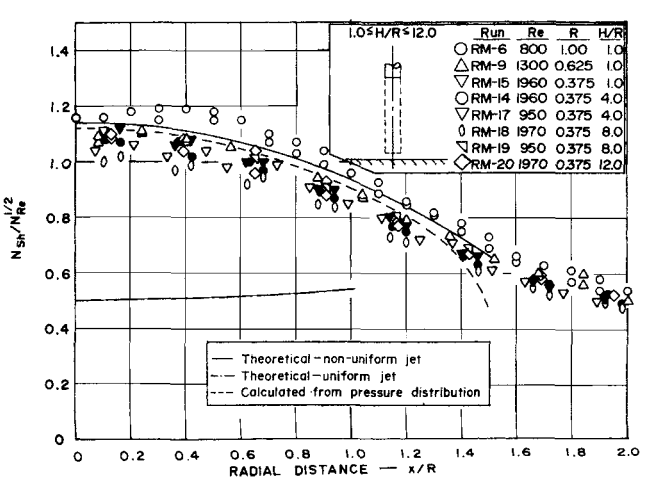

Fig. 3. Mass transfer data in impingement region, $1.0 \leq H/R \leq 12.0$, $N_{Sc} = 2.45$. Comparison with theory.

TABLE 1. TABULATION OF THE APPROXIMATE GENERALIZED FORM OF THE SOLUTION FOR MASS TRANSFER IN AN IMPINGING JET FOR SCHMIDT NUMBERS IN THE RANGE 1.0 TO 10.0

$$N_{Sh}/N_{Re}^{1/2} = a\,N_{Sc}^{0.361} + b\,N_{Sc}^{0.368}\,(x/R)^2 + c\,N_{Sc}^{0.408}\,(x/R)^4 + d\,N_{Sc}^{0.424}\,(x/R)^6 + e\,N_{Sc}^{0.433}\,(x/R)^8 + f\,N_{Sc}^{0.439}\,(x/R)^{10} + g\,N_{Sc}^{0.442}\,(x/R)^{12}$$

H/R	a	b	c	d	e	f	g
1.0	0.8242	-1.351×10^{-1}	-9.850×10^{-3}	1.171×10^{-3}	2.856×10^{-4}	2.458×10^{-6}	-6.352×10^{-7}
0.5	0.8269	-1.329×10^{-1}	-1.004×10^{-2}	5.694×10^{-4}	1.360×10^{-4}	-1.871×10^{-5}	-4.469×10^{-6}
0.375	0.8177	-1.150×10^{-1}	6.297×10^{-2}	5.684×10^{-2}	1.370×10^{-3}	-2.348×10^{-2}	-1.867×10^{-2}
0.25	0.8301	-1.642×10^{-2}	1.033×10^{-1}	4.682×10^{-3}	-2.613×10^{-2}	-6.034×10^{-3}	-5.345×10^{-3}
0.10	0.8436	7.368×10^{-2}	5.298×10^{-1}	4.903×10^{-1}	-6.312×10^{-2}	-4.664×10^{-1}	-1.503

The functions $d'_4(\eta)$ and $e'_4(\eta)$ depend only on η and the Schmidt number. Thirty such functions are involved in evaluating the first seven terms of Equation (20). These functions are tabulated elsewhere (3); the other six linear expressions analogous to Equation (21) are also given.

Performing the calculations for a Schmidt number of 2.45 (naphthalene-air) the present nonuniform jet with $H/R = 1.0$ gives,

$$\frac{N_{Sh}}{N_{Re}^{1/2}} = 1.144 - 0.1923\left(\frac{x}{R}\right)^2 - 0.01453\left(\frac{x}{R}\right)^4 + 0.001606\left(\frac{x}{R}\right)^6 + \ldots\ldots \quad (22)$$

This expression is specific for $N_{Sc} = 2.45$. An approximate method of expressing the gradients such as $d'_4(0)$, $e'_4(0)$ ... explicitly in the terms of the Schmidt number is given (3). Using this approximate method, Equation (20) becomes:

$$\frac{N_{Sh}}{N_{Re}^{1/2}} = a\,N_{Sc}^{0.361} + b\,N_{Sc}^{0.386}\left(\frac{x}{R}\right)^2 + c\,N_{Sc}^{0.408}\left(\frac{x}{R}\right)^4 + \ldots\ldots \quad (23)$$

In this approximate form of the solution the Schmidt number is explicitly included. The values of the coefficients a, b, ... in Equation (23) given by this approximation have been calculated for the nonuniform impinging jet for H/R values in the range 0.1 to 1.0; these coefficients were obtained for Schmidt numbers in the range $1.0 \leq N_{Sc} \leq 10.0$. Using (3) coefficients for the Schmidt number ranges from 10 to 100 and 100 to 1,000 can also be calculated. Since the accuracy of the approximation given by Equation (23) is dependent on the convergence of the series an accuracy check should be made using the exact series.

In a similar manner the mass transfer from the impingement surface using a uniform impinging jet can be calculated using the boundary layer solution and the four terms of the inviscid solution calculated by Strand (4) for $H/R = 2.0$ [shown as Equation (28) in Part I], giving

$$\frac{N_{Sh}}{N_{Re}^{1/2}} = 0.3634\,N_{Sc}^{0.361} + 0.03441\,N_{Sc}^{0.386}\left(\frac{x}{R}\right)^2 - 0.002531\,N_{Sc}^{0.408}\left(\frac{x}{R}\right)^4 - 0.001741\,N_{Sc}^{0.424}\left(\frac{x}{R}\right)^6 \quad 1 \leq N_{Sc} \leq 10 \quad (24)$$

This approximate form agrees with the exact form to within 0.5% for $x/R \leq 1.0$.

Figure 2 is a plot of the exact solutions such as Equation (22) which are given in the literature (3) and the approximate forms given by Equation (23) and Table 1. Equation (24) for the uniform impinging jet is also plotted. The dimensionless group $N_{Sh}/N_{Re}^{1/2}$ is plotted vs. x/R. For $H/R = 1.0$, 0.5 and 0.375 the approximate solution shows good agreement with the exact form with less than 0.5% error for $H/R = 1.0$ and 0.5. At lower nozzle clearances, $H/R = 0.25$ and 0.1, the series solution converges less rapidly and for $x/R > 0.9$ and 0.8 respectively, errors incurred by using the approximate solution become appreciable.

Examining the variations of mass transfer with radial distance shown in Figure 2 for various nozzle elevations, it is seen that in all cases the mass transfer rate near the stagnation point, $x/R < 0.2$ shows little dependence on radial distance. This result is in accord with the finding of Yih (5) who has shown that heat transfer coefficients near an axisymmetric stagnation point are independent of radial distance. Hence, for small radial distances, mass transfer calculations may be made using only the first term of Equation (23); this term in Table 1 is independent of H/R within the limits of accuracy of the numerical procedures of Part I. For radial distances greater than $0.2R$, the effects of nonuniformity in the jet and nozzle height become appreciable. For $H/R \geq 0.5$ the mass transfer for $x/R > 0.2$ decreases monotonically with radial distance; for $H/R = 0.375$ a second maximum in the mass transfer curve occurs near $x/R = 1.0$ due to the presence of the nozzle. The curves for $H/R = 0.25$ and 0.1 show rapid increases in transfer rate as the nozzle wall, $x/R = 1.0$, is approached.

Equation (24) plotted in Figure 2 shows that the transfer coefficient in the stagnation region of a uniform impinging jet increases only slightly with radial distance. It can, therefore, be inferred from these calculations that for $x/R \leq 1$, flow in the uniform impinging jet is a fair approximation to classical axisymmetric stagnation flow.

EXPERIMENTAL PROCEDURE

Point mass transfer coefficients were obtained in the stagna-

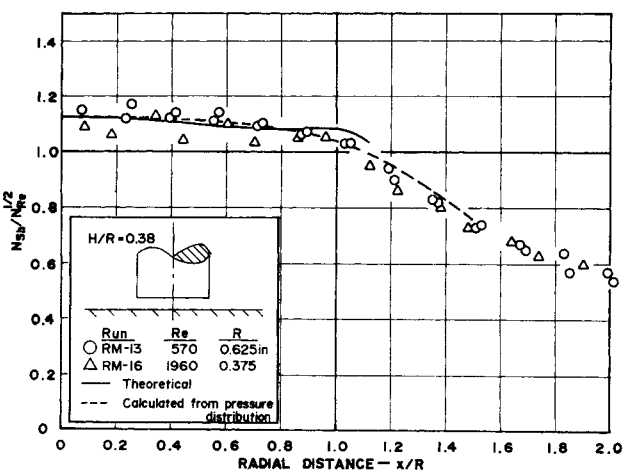

Fig. 4. Mass transfer data in impingement region, $H/R = 0.38$, $N_{Sc} = 2.45$. Comparison with theory.

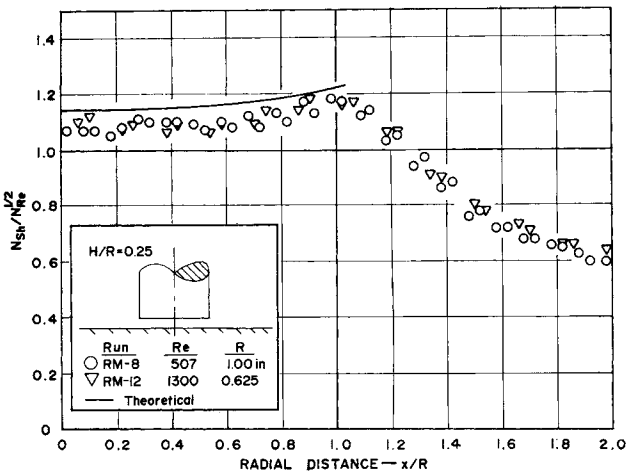

Fig. 5. Mass transfer data in impingement region, $H/R = 0.25$, $N_{Sc} = 2.45$. Comparison with theory.

tion region of a laminar jet of air originating with fully developed laminar pipe flow. From measurements of the local sublimation rates of a naphthalene coating exposed to the air jet, local mass transfer coefficients and Sherwood numbers were calculated.

Equipment

The experimental equipment comprising nozzle and impingement surface was identical to that used for velocity and pressure measurements described in Part I of this paper.

For mass transfer measurements, a separate impingement surface 8 × 8 in. was placed on the larger plane surface. This smaller plate was coated with a film of naphthalene, the thickness profile of which was measured before and after exposure of the surface to the impinging jet for a time period of up to 20 hr. Surface thickness profiles were measured using a bridge and mechanical gauge which was read to 0.0001 in. Maximum thickness decrease during a run was about 0.015 in. The accuracy of sublimation rates measured in this manner is estimated to vary from ± 2% at the stagnation point to ± 6% at x/R = 2.

The temperature of the naphthalene coating was continuously recorded by a thermocouple embedded in the coating; sublimation rates were low and surface temperature variations due to sublimation were negligible. Experiments were carried out in a constant temperature room to avoid natural convection and other thermal gradient effects.

Coating procedure

The method of applying the naphthalene film to the plate was found to be of importance for obtaining accurate and reproducible data. The plate was inclined at about 30 deg. to the horizontal. Molten naphthalene at 120°C. was poured onto the plate at the upper edge so that excess liquid drained from lower edge of the surface. Heat was absorbed from the liquid by the plate, and a film of naphthalene about 0.05 in. thick was deposited. Such a film required a minimum amount of mechanical smoothing; during a run the coating remained smooth and the reproducibility of data was good. Coatings prepared by allowing molten naphthalene to solidify on a horizontal surface gave rough and pitted surfaces on sublimation and results were erratic (3); large crystals were evident in this type of coating. The former coating method was used for all mass transfer work reported.

Calculation of results

The local thickness decrease data, coating temperature, and run time were used to calculate the mass transfer coefficients from:

$$k = \frac{\Delta t}{\theta} \frac{\rho_s}{c_s} \qquad (25)$$

The coating density measured using a liquid density gradient column was 1.08 g./cc.; there was no significant variation in coating density from run to run. The vapour pressure of naphthalene was obtained elsewhere (6). Sherwood numbers were calculated from the mass transfer coefficients using a value of 0.0611 sq. cm./sec. for the diffusivity of naphthalene in air (7).

RESULTS AND DISCUSSION

Sublimation mass transfer data were taken in the stagnation region of a nonuniform impinging jet for the naphthalene-air system ($N_{Sc} = 2.45$). The ranges of variables used were: $0.1 \leq H/R \leq 12.0$; $500 \leq N_{Re} \leq 1{,}960$ and 0.75 in. $\leq D \leq 2.0$ in.; these data are shown in Figures 3 to 6 where the dimensionless group $N_{Sh}/N_{Re}^{1/2}$ has been plotted vs. x/R in accordance with Equation (22). Data covering the wall-jet region out to $x/R \leq 14$ have also been obtained; these data are shown in Figures 7 and 8. The run numbers given in the legend of these figures refer to (3).

Data for $1.0 \leq H/R \leq 12.0$

Mass transfer runs for nozzle heights up to $12R$ are plotted in Figure 3. The upper solid curve is the predicted mass transfer calculated from Equation (22) for $H/R = 1.0$. The experimental data show a random scatter of ± 10% but on an averaged basis the agreement with theory for $x/R \leq 1.5$ is good. The theoretical mass transfer curve is about 4% above the averaged experimental data. Referring to Part I of this paper and noting the invariance of experimental pressure distributions for $1.0 \leq H/R \leq 12.0$, it would be anticipated that mass transfer rates would similarly depend very little on nozzle elevation in this range. The data in Figure 3, within the limits of experimental error, show no dependence on H/R.

The broken curve in Figure 3 is the mass transfer predicted from the experimental pressure distributions shown in Part I of this paper. The velocity at the edge of the boundary layer was calculated from the pressure data for $H/R = 1.0$ and the coefficients u_1, u_2 .... in Equation (5) were obtained by least squares fitting. This semi-empirical curve is slightly lower than the theoretical prediction and is about 2% higher on the average than the experimental data; hence, it would appear that in the absence of a theoretical description of the impinging jet pressure distribution data may be used with good accuracy for mass transfer calculations in an impinging jet.

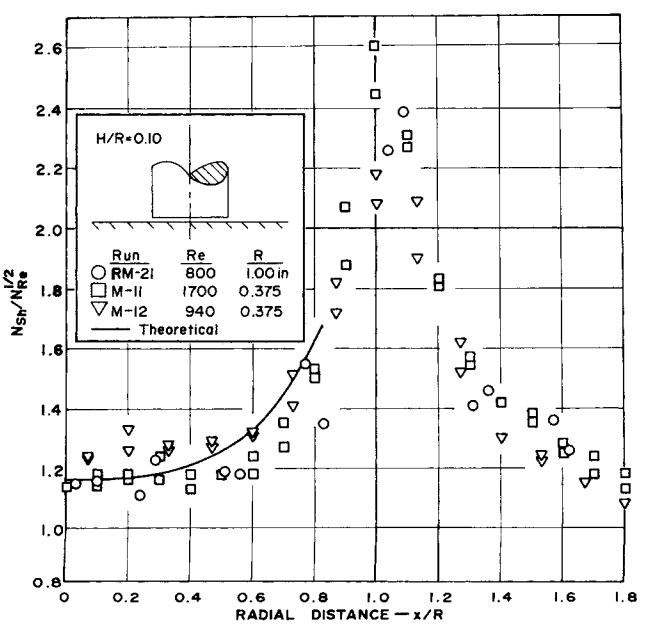

Fig. 6. Mass transfer data in impingement region, $H/R = 0.1$, $N_{Sc} = 2.45$. Comparison with theory.

The lower broken curve in Figure 3 is the mass transfer which is predicted for the uniform impinging jet, Equation (24). No experimental mass transfer data using a uniform jet were taken; the accuracy of this theoretical curve, however, can be inferred from the good agreement between pressure distributions calculated from Strand's inviscid solution for the uniform jet and measured data of Ludwig and Brady (*1*). In view of present experience where mass transfer measurements agree well with calculations based on experimental pressure distribution data, the curve shown in Figure 3 is thought to be quite reliable.

Comparison of the mass transfer predicted for the uniform impinging jet with that presently obtained for a parabolic velocity distribution shows the latter to be higher by a factor of 2.2 at the stagnation point, decreasing to a factor of 1.6 at $x/R = 1.0$. This comparison is based on equal nozzle Reynolds numbers. Based on equal axial velocities in the jet, the nonuniform jet stagnation-point transfer is a factor of 1.65 higher than that for a uniform jet.

For small radial distances,

$$U(x) = u_1 x \tag{26}$$

and, therefore, in the vicinity of the stagnation point,

$$\frac{-d^2p}{dx^2} = u_1^2 \tag{27}$$

where the coefficient u_1 is directly related to the stagnation-point mass transfer rate, Equations (5) and (19). It can readily be deduced from the curvature of the pressure distributions for the uniform and nonuniform jets shown in Figure 6, Part I, that the radial acceleration of fluid in the stagnation region is much higher in the latter jet; the higher mass transfer rate shown in Figure 3 for the nonuniform jet is a direct result of this increased acceleration.

Data for H/R ≤ 1.0

Mass transfer data for $H/R = 0.375$, 0.25, and 0.1 are shown in Figures 4 and 5; data for $H/R = 0.5$, 5, and 6 have also been taken and are given in (*3*). The data for $H/R = 0.5$ (not shown) cannot be distinguished from those shown in Figure 3 for $H/R \geq 1.0$; this is in agreement with the theoretical results plotted in Figure 2.

For $H/R < 0.5$, the experimental data clearly show the effect of nozzle-to-surface clearance. The mass transfer data for $H/R = 0.375$ shown in Figure 4 conform in trend to the theoretical curve; however, the second maximum due to the nozzle wall at $x/R \approx 1.0$ predicted by theory is not apparent. Also shown as a dotted line is the mass transfer

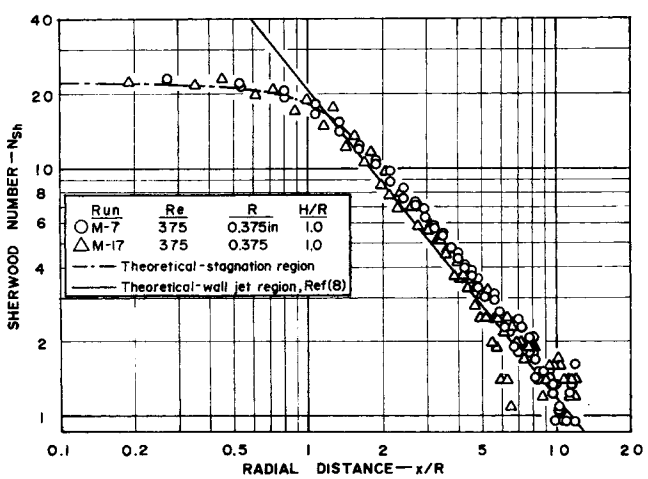

Fig. 7. Mass transfer in the stagnation and wall jet regions, N_{Re} = 375, N_{Sc} = 2.45. Comparison with wall jet theory.

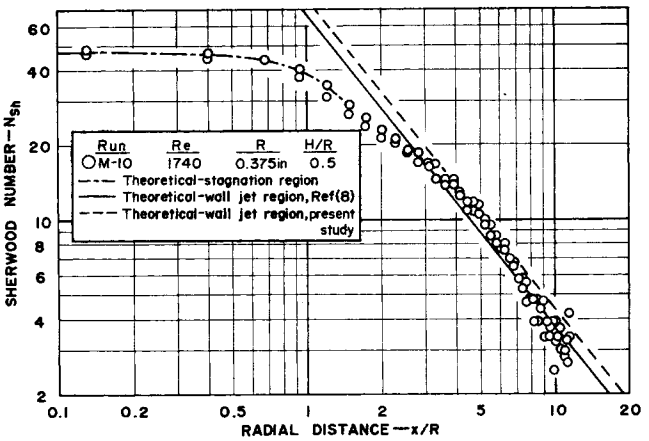

Fig. 8. Mass transfer in the stagnation and wall jet regions, N_{Re} = 1,740, N_{Sc} = 2.45. Comparison with wall jet theory.

curve calculated from the measured pressure distribution; this curve shows good agreement with the experimental data and the theoretical curve. A maximum in the rate of transfer is shown clearly by the data for $H/R = 0.25$ in Figure 5.

The data for $H/R = 0.1$ are given in Figure 6. The effect of the nozzle wall is clearly evident from these data. The transfer rate rapidly increases with radial distance out to $x/R \approx 1.0$ where it is about twice the stagnation-point value; with a further increase in x/R, the transfer rate decreases. The maximum rate shown in Figure 6 corresponds to the region of maximum radial velocity as the fluid passes under the nozzle wall. The theoretical curve which is valid for $x/R < 0.8$ is also shown in Figure 6; there is good agreement with experiment.

Transition to wall jet mass transfer

From the present investigation of stagnation region mass transfer an expression which adequately correlates the experimental data may be written in the form

$$N_{Sh} = f\left(N_{Sc}, \frac{x}{R}\right) N_{Re}^{1/2} \quad \text{(stagnation region)} \tag{28}$$

The equivalent expression for mass transfer in the laminar radial wall-jet from (*8*) is:

$$N_{Sh} = 0.5071 N_{Re}^{3/4} \left(\frac{x}{R}\right)^{-5/4} [-g^1(0)] \quad \text{(wall jet region)} \tag{29}$$

where $[-g^1(0)]$, a function of the Schmidt number only, is the dimensionless concentration gradient at the wall; for $N_{Sc} = 2.45$ this function has the value 0.479.

Since the dependence of mass transfer on Reynolds number differs in the stagnation and wall-jet regions, the relationship between the mass transfer in these two regions on a plot of N_{Sh} vs. x/R will depend on N_{Re}. For $N_{Re} = 375$, the two theoretical predictions, shown in Figure 7, intersect at $x/R = 1.2$, and the combination of Equations (28) and (29) covers the entire x/R range. The data conform to the stagnation-region theory for $x/R \leq 1.2$ and to wall-jet theory for $x/R \geq 1.2$. The entire range of radial distances is, thus, accounted for in terms of theory.

At higher Reynolds numbers, that is $N_{Re} = 1{,}740$, the two mass transfer expressions, Equations (28) and (29) do not intersect (Figure 8) and there is a range of x/R for which mass transfer is not accounted for by present theory. Outside of this range, $x/R \leq 1.5$ and ≥ 3 the data shown in Figure 8 agree well with stagnation theory and wall-jet theory, respectively. Within the range $1.5 \leq x/R \leq 3$ the

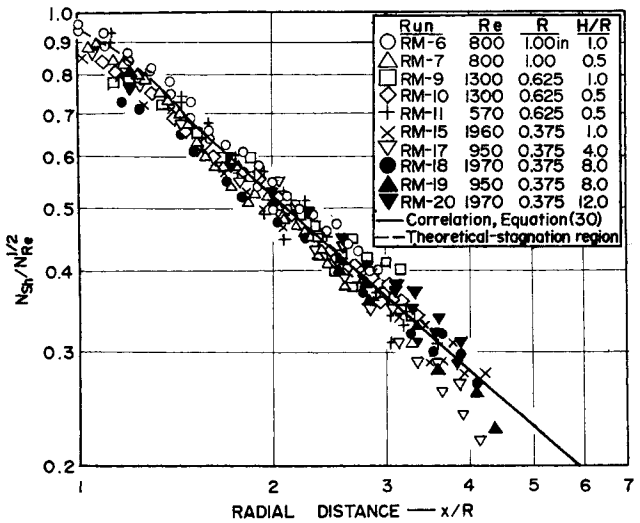

Fig. 9. Correlation of mass transfer data in transition region, $N_{Sc} = 2.45$.

experimental data indicate a smooth transition from stagnation flow to wall-jet flow. This transition might be rationalized in terms of an impingement region theory covering this x/R range. In the absence of such theoretical results this x/R range will be regarded as a region of change from impingement flow to the laminar wall-jet boundary layer. Data in the transition region can be correlated in terms of $N_{Re}^{1/2}$; Figure 9 shows these data for Reynolds numbers in the range 570 to 1,970 and for $1 \leq x/R \leq 4.5$; $N_{Sh}/N_{Re}^{1/2}$ has been plotted vs. x/R. The data are well correlated by the equation

$$\frac{N_{Sh}}{N_{Re}^{1/2}} = 0.95 \left(\frac{x}{R}\right)^{-0.86} \quad \text{for} \quad x/R \geq 1.5 \quad (30)$$

The intersection between this correlation and the theoretical wall-jet line depends on N_{Re} and gives the upper x/R limit for Equation (30).

SUMMARY AND CONCLUSIONS

Theoretical calculations of local mass transfer coefficients in the impingement region of a jet with a parabolic velocity profile have been compared with sublimation mass transfer data for the air-naphthalene system. The laminar boundary layer calculations were carried out with boundary conditions from an inviscid solution for the impingement region and also for boundary conditions from experimental pressure distribution data. The agreement between experiment and theory is good in all cases.

For nozzle-to-surface distances in the range 0.5 to 12R mass transfer from the impingement surface is independent of nozzle distance. With the nozzle closer to the surface ($< 0.5R$) there is no significant change in the transfer rate near the stagnation point ($x/R < 0.2$); at larger radial distances, however, the constriction of flow between the nozzle and the impingement surface causes the transfer rate to increase with decreasing nozzle height.

Mass transfer data taken outside the impingement region agree well with wall-jet theory for Reynolds numbers less than 550. At higher Reynolds numbers an intermediate region between present impingement theory and laminar wall-jet theory is apparent from the data. An empirical correlation of data in this transition region is proposed.

From theoretical calculations for the uniform impinging jet it is inferred that, for equal nozzle Reynolds numbers, mass transfer at the stagnation point is less than half that observed for the present nonuniform jet. This is attributed to a lower flow acceleration in the stagnation region of the uniform jet.

ACKNOWLEDGMENT

Financial assistance from the National Research Council of Canada is gratefully acknowledged.

NOTATION

A_{2n} = constant coefficients from inviscid solution, Part I
c = concentration of diffusing species, g./cc.
$\bar{c}$ = dimensionless concentration
c_s = saturation concentration of solute, g./cc.
$c_0(\eta)$, $c_2(\eta)$ ... = functional coefficients in series solution, Equation (17), cm.^{0}, cm.$^{-2}$ .....
D = nozzle diameter, cm.
$\mathcal{D}$ = solute diffusivity, sq.cm./sec.
$f_1(\eta)$, $f_3(\eta)$ .... = functional coefficients in series solution, Equation (12)
H = nozzle-to-surface distance, cm.
k = mass transfer coefficient, cm./sec.
N_0 = mass flux at the wall, g./sq.cm.-sec.
p = pressure, dynes/sq.cm.
R = nozzle radius, cm.
$\mathcal{R}'_n(0)$ = wall values of functions from inviscid solution, Part I
u = component of velocity in x-direction, cm./sec.
$U(x)$ = characterizing velocity at edge of boundary layer, cm./sec.
U_N = axial velocity in nozzle, cm./sec.
$\bar{U}$ = average velocity in nozzle, cm./sec.
u_1, u_3 ..... = constants defined by Equation (5), sec.$^{-1}$, sec.$^{-3}$, ...
v = component of velocity in y-direction, cm./sec.
x = cylindrical coordinate in radial direction, cm.
y = cylindrical coordinate normal to impingement surface, cm.

Greek Letters

Δt = thickness decrease of coating, cm.
$\vec{\zeta}$ = vorticity vector, sec.$^{-1}$
η = dimensionless distance from impingement surface
θ = run time, sec.
ν = kinematic viscosity, sq.cm./sec.
ρ = density, g./cc.
ρ_s = coating density, g./cc.
ψ = stream function, sq.cm./sec.

Dimensionless Groups

N_{Sh} = Sherwood number, $kR/\mathcal{D}$
N_{Re} = Reynolds number, $\bar{U}D/\nu$
N_{Sc} = Schmidt number, $\nu/\mathcal{D}$

LITERATURE CITED

1. Brady, W. G., and G. Ludwig, *Inst. Aerospace Sci., Paper No. 63-29* (1963).
2. Schlichting, H. "Boundary Layer Theory" 4th Ed. Chapt. X, XIV, McGraw-Hill, New York (1960).
3. Scholtz, M. T., Ph.D. dissertation, Univ. Toronto, Canada (1965).
4. Strand, T., *Am. Inst. Aeron. Astronaut. Paper No. 64-424* (1964).
5. Yih, C-S., *J. Aeron. Sci.*, 21, 37 (1954).
6. Sherwood, T. K., and H. S. Bryant, Jr., *Can. J. Chem. Eng.*, 35, 51 (1957).
7. "International Critical Tables" McGraw-Hill, New York (1928).
8. Scholtz, M. T., and O. Trass, AIChE J., 9, 548 (1964).

Manuscript received March 26, 1968; revision received July 12, 1968; paper accepted July 15, 1968.